[Research Note]

Snail Density Estimation for Schistosomiasis Control by Integrating Field Survey and Multiscale Satellite Images

Bing Xu[1], Peng Gong[2], Song Liang[3], Edmund Seto[3] and Bob Spear[3]

[1]Department of Geography, Texas State University, San Marcos, Texas 78666
[2]Center for Assessment and Monitoring for Forest and Environmental Resources, University of California, Berkeley, CA 94720-3110
[3]School of Public Health, University of California, Berkeley, CA 94720

I. INTRODUCTION

In a mountainous region of Sichuan Province, China, snails live along the edges of ditches in crop fields. People are infected through contact with the contaminated waters of natural rivers and irrigation systems. Infected human and animal stools are used as fertilizers in the crop fields, from which the disease can also be transmitted. Snail population is crucial for more refined analysis of schistosomiasis transmission and for the development of a control model. We focus on five land-use and land-cover categories to which the snail habitat and the water exposure activities of humans may be closely related. These are lowland crop, upland crop, terraced crop field, riverbed and residential area.

Surrounding Qionghai Lake at the southern edge of Xichang City, Sichuan Province, our study site resides in the valley of a mountainous area of western China with an elevation range of 1500-2500 m. A multispectral IKONOS image of the study site was acquired in December 2000, covering an area of 137 km^2 (Figure 1). The spatial resolution of the image is 4 m (Space Imaging, 1999). The study site consists of approximately 200 residential groups organized into 4 townships. The climate there is subtropical with an annual average temperature of 17 °C and an annual rainfall of about 1000 mm, over 90% of which falls between the beginning of June and the end of October. The main agricultural products are rice, corn, wheat, bean, garlic, rape, eggplant and tomatoes (Spear, et al., 1998). Most people are farmers, and secondarily, raisers of livestock and fish. People get infected when they come into contact with infected water. They might be growing crops and vegetables in the lowland, the upland fields or terraced areas, washing their feet and working utensils along the ditches where the irrigation system runs or playing in the riparian zones along riverbeds.

II. DATA PREPROCESSING

The IKONOS image is georeferenced to UTM projection based on the 1984 World Geodetic System. We then treat the geometrically corrected IKONOS scene as the master image, and four other satellite images are geo-matched accordingly. The four registered images include Landsat TM data taken in March 1998 and November 1998, EO-1 ALI and Hyperion data taken in January 2002.

We apply regression analysis to the reference data for the five land-use categories. On the one hand, we want to assess the capability of the Landsat Thematic Mapper (TM), EO-1 Advanced Land Imager (ALI) and Hyperion to extend local-scale knowledge to large-scale monitoring of the disease transmission. However, land parcel size in this study area is often smaller than the 30m by 30m pixel of the Landsat or EO-1 data. Extracting land surface cover information at sub pixel levels thus becomes important. We use classification results from the multispectral IKONOS imagery as "ground truth" data. Landsat and EO-1 data are used as regressors after geometric registration of these satellite images. The proportions of those land surface covers are subsequently estimated.

III. LAND COVER CLASSIFICATION WITH IKONOS AND ELEVATION DATA DERIVED FROM ASTER DATA

Elevation in this mountainous schistosomiasis endemic area is important, as prevalence in the upland regions is higher than in the lower floodplains. People may grow very different agricultural products in the lower and upper lands. Therefore, upland and lowland crop and terraced area are distinct land surface categories. The land-cover classification map is made by extracting the lake separately and including elevation data in the classification of IKONOS multispectral imagery. The lake delineation was achieved by processing the near-infrared (NIR) channel (band 4) of the IKONOS imagery. The first step of the processing procedure is applying a Sobel filter to the NIR image to enhance the contrast between water and land. A Sobel filter is an edge-enhancement technique that calculates from a 3 X 3 neighborhood the vertical and horizontal gradients and takes the square root of their sum of squares (Jensen, 1996). A 5 X 5 average filter was applied to the edge-enhanced

1082-4006/03/0901~2-97$5.00

Figure 1. Study site in Xichang, Sichuan, China in a false color composite of the IKONOS CARTERRA imagery taken in December 2000. Yellow color represents snail survey sites in 19 residential groups.

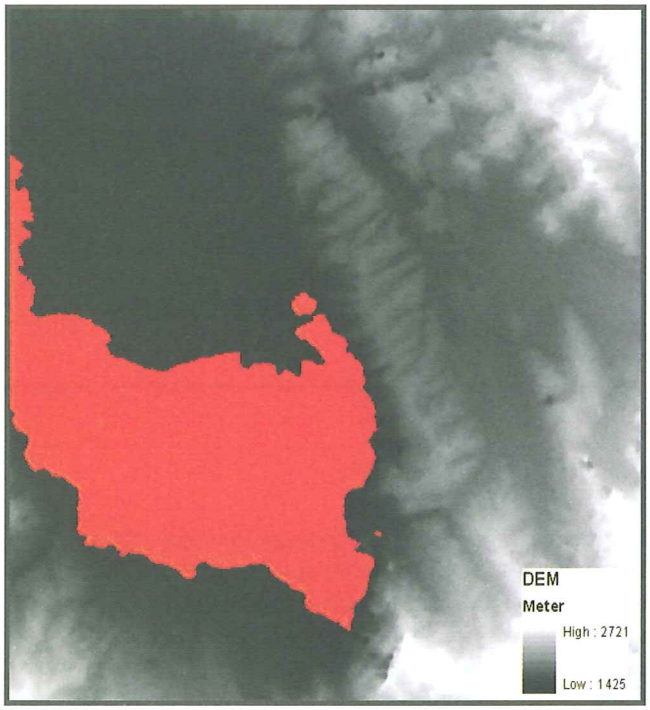

Figure 2. Resultant lake mask in red with the digital elevation model (DEM) displayed in the background. The lake mask is generated by thresholding a Sobel filtered near-infrared IKONOS image followed by region growing and editing. The DEM is generated from a stereopair of ASTER images in an original resolution of 15 m. It has been resmapled to 4 m for the purpose of image classification.

image to produce an edge-density image. This effectively removed a large number of shaded land areas in the NIR image from being subsequently labeled as water bodies. It also prevented a large number of fishponds from being processed as lake. For the next step, a threshold is empirically determined from the histogram of the enhanced image to threshold out those low gradient areas as a mask of water bodies. Because of the edge-effect of the Sobel and averaging filtering techniques, the detected mask of water bodies is smaller than it ought to be by 2 pixels around the borders. A region growing morphological filtering procedure was then applied to the mask twice to ensure proper restoration of the water bodies. Some editing is performed on the water-body mask to remove non-water body or fishpond portions in the image. This edited mask is then used as a mask to be excluded during subsequent land-cover and land-use classification (Figure 2). The precise extraction of the lake category from the NIR image makes it unnecessary to keep the original lake edge whose spectral properties are different from the central part of the lake.

Before the inclusion of elevation in the land-cover and land-

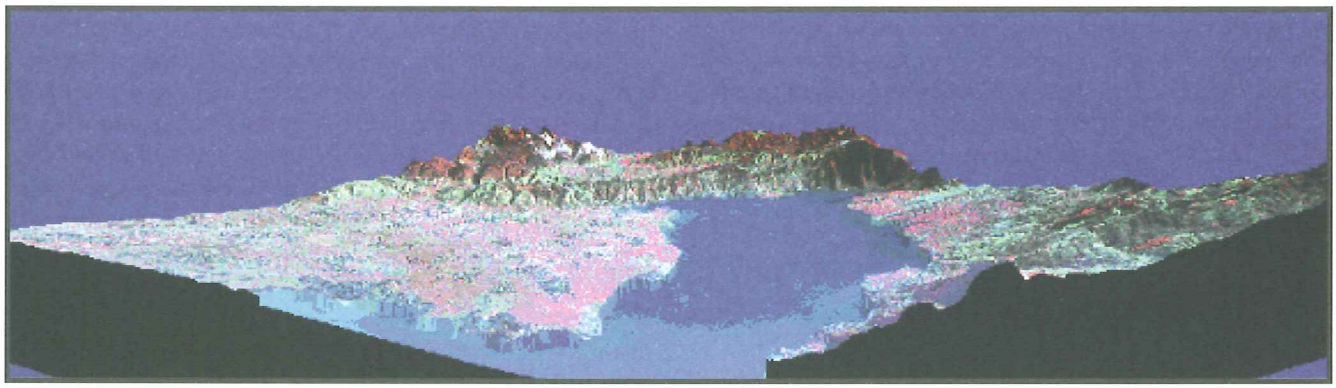

Figure 3. Color infrared composite of the IKONOS draped over the DEM as viewed from the west side of the study area to the east from an elevation of 10,000 m.

use classification, there was some confusion among various classes, particularly between the lowland crop and upland crop, and between shadowed areas and the residential areas. These errors are substantially reduced with the inclusion of a digital elevation model (DEM) layer in the classification. The DEM was produced using PCI's Orthoengine software applied to a stereopair of ASTER images acquired in August, 2002. ASTER stands for Advanced Space-borne Thermal Emission and Reflection Radiometer. It is a Japanese instrument on board of the Terra satellite launched in December 1999. ASTER has visible, NIR and thermal channels with various ground resolutions. Its stereopair is taken from nadir and backward looking directions along the same track using the 0.7-0.9 mm wavelength band with a ground resolution of 15 m. At our study area, we did accuracy assessment using 29 GCPs measured with differential GPS. The average root-mean squared error is only 6.1 m. This does not affect the results of this study because we use DEM to distinguish the upland and lowland crops whose elevation difference exceeds 100 m. Figure 3 shows a perspective view of the study site by draping the color-infrared composite of the IKONOS image over the DEM. The lake water level was not measured through digital photogrammetry. It was set to an estimated value. From the perspective view it can be seen that the pre-set value was not correct. The actual lake level should be greater than the estimated value. Because the lake area was excluded in this study, we did not further adjust the lake surface elevation.

Land-cover and land-use classification is performed over the land area with modified training samples applied in a maximum likelihood classification algorithm. As a result, a total of 15 classes is mapped (not including the Lake and the abolished lake edge class). Some preliminary studies in this area done by Robert Spear's group in the School of Public Health and Xueguang Gu's group in Sichuan, China suggest that type of crop field plays an important role in schistosomiasis transmission. Therefore, attention is paid to these classes as well as to residential and sandy river beds. Although forest, lake, shrub and barren mountain top occupy a large proportion of the mapped area, they are not considered important schistosomiasis transmission sites. The overall accuracy of 15 land surface categories is 0.865 measured by Kappa coefficient. For example, the accuracies for the residential, river beds, lowland crop, lowland terrace, upland crop and upland terrace are 87% (out of 2125 samples), 91% (out of 4469 samples), 98% (out of 751 samples), 89% (out of 3134 samples), 97% (out of 1193 samples), and 98% (out of 2101 samples), respectively.

IV. LAND COVER FRACTION ESTIMATION

The EO-1 Hyperion is the only hyperspectral sensor operating in space (NASA, 1996). A hyperspectral sensor has contiguous narrow wavelength bands (about 10 nm each) that are supposed to capture more subtle spectral details of the objects on the ground than can the bands (about 100 nm each) of a multispectral sensor. However, the quality of some of the bands, particularly water vapor absorption bands, may be degraded due either to insufficient energy within the narrow wavelength band captured by the sensor or to the disturbance of water absorption. Striping appears in some of the bands. Problems are encountered with direct use of either a hyperspectral image or feature reduced images. Statistical estimation from noisy bands can be unreliable. During the process of feature reduction the high variability of the noise, especially the striping behavior, is mistakenly treated as variability of the signals and, under the assumption that the noise has typically equal and low variability, preserved within the principal components. We proposed a way of recovering the original Hyperion spectral space by properly estimating the noise structure, inverting a transformation matrix of the noise adjusted PCA and the first ten principal component images (Xu, 2003)

It is often difficult to process such high-dimensional data typically more than 200 bands. It causes a heavy computational burden. The limited number of training samples, compared to the high dimension of the data, and the high correlation among adjacent bands leads to inaccurate estimation of the covariance structures and to degenerate ranks of spectral matrices, thus limiting the accuracy of classification and regression in our case. Due to complexities caused by the high dimensional space, feature extraction schemes such as the Efroymson stepwise procedure (ESP), PCA and nested selection regression (NSR) have been applied to minimize regression errors, reducing high-dimensionality either by implementing stepwise selection and deletion of bands or by maximizing the ordered variance of the whole data set. Land-use fraction estimation results using the resultant reduced features are compared with those using all the original spectral bands.

Linear spectral unmixing is a technique commonly applied, particularly with hyperspectral data, to derive end member proportions from within each pixel of remotely sensed imagery (Gong et al., 1994). We compared Ordinary Least Squares (OLS) with a linear unmixing model in terms of both mathematical formulation results and experimental estimation results. While the two methods produced similar unmixing results, the OLS produced smaller error.

V. SNAIL DENSITY ESTIMATION

Surface cover fractions derived from 30 m resolution satellite data are then used in a multiple regression to estimate snail densities of an area covering approximately 200 villages. Nineteen villages have been under our intensive investigation for the past three years. A ditch network for each of the 19 groups was constructed by using a differential Global Positioning System (GPS) in the summer of 2000. At the same time a snail survey was done every 10 m along the ditches of all 19 residential groups (Figure 1). Altogether 10,558 sites were visited for snail survey. For each site, the number of snails was counted and positive snails were examined and

counted within a kuang, which is a frame occupying 0.11 m^2 area. Among these sites, 3157 sites were found to have snails and 7401 sites did not. Among the snail sites, 93 sites were found to have positive snails.

As presented above, to assess the capability of Landsat and EO-1 sensors for larger scale monitoring, IKONOS classification result served as ground truth. The land-cover types were designed in this classification so that the end results were not sensitive to seasonality and we think they have not changed in the past several years. Whenever we have a 30 m by 30 m Landsat or EO-1 pixel, we are able to derive the area proportion of each land-cover type within this pixel by using the IKONOS data. We apply the same concept here. For each snail survey site, we place a transparent 30 m by 30 m mask over the improved 4 m by 4 m land-cover map produced by a multispectral IKONOS image and elevation data. This way, we have snail survey data together with 15 land-cover fractions for each site under investigation. A prediction model is then built based on snail surveys from the summer of 2000 at more than 10,000 sites over 19 land groups and their corresponding land-cover fractions. $\hat{SA} = \hat{a}_1 f_1 + \hat{a}_2 f_2 + \cdots \hat{a}_i f_i \cdots + \hat{a}_k f_k$. k is the number of land-cover classes selected for prediction. $\hat{SA}$ denotes snail abundance to be predicted at each site, $\hat{a}_i$ and f_i, $i = 1, 2, \ldots k$, are estimated model coefficients and calculated land-cover fractions, respectively.

After significance tests and careful assessment of the individual categories, thirteen out of fifteen land-cover and land-use categories were selected for predictions of snail abundance and seven were selected for prediction of positive snail abundance. Lake and forest were removed from the prediction models as the two categories are totally insensitive to snail abundance. Since our focus is not on the prediction of snail abundance at each site at the 10-30 m scale but instead at the village level, it is important for us to assess the prediction results against the aggregated results within the territory of each of the surveyed residential groups. Figure 4 shows that the best snail density prediction results with an R^2 of 0.86.

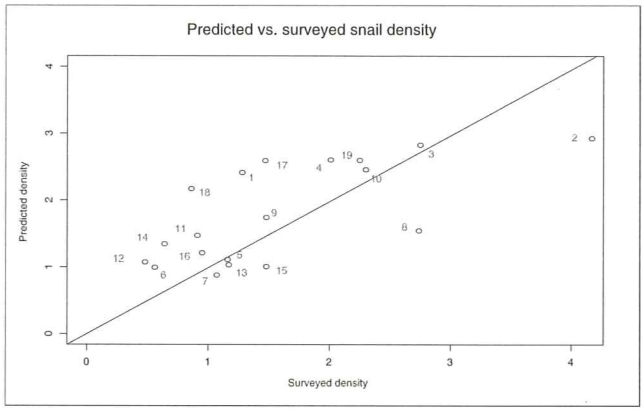

Figure 4. Estimated snail density against field surveyed snail density. Each of the 19 groups is labeled. Regression line has a slope of 0.99, close to 1.

ACKNOWLEDGEMENT

This research was supported by Foundamental Basic Science Grant (2001CB3094) and an NIH grant.

REFERENCES

[1] Gong, P., J.R.Miller, and M. Spanner, 1994. Forest canopy closure from classification and spectral unmixing: a multi-sensor evaluation of application to an open canopy, *IEEE Trans. on Geos. and Remote Sens.* 32(5): 1067-1080.

[2] Jensen, J.R., 1996. *Introductory Digital Image Processing: A Remote Sensing Perspective,* Prentice Hall, Englewood Cliffs, N.J.

[3] Spear, R., P. Gong, E. Seto, B. Xu, Y. Zhou, D. Maszle, S. Liang, G. Davis, X. Gu, 1998. GIS and remote sensing for schistosomiasis control in Sichuan, China, *Geographic Information Sciences*, 4(1-2): 14-22.

[4] Xu, B., 2003. Spatio-temporal modeling with GIS and remote sensing for schistosomiasis control in Sichuan, China, Doctoral Dissertation, Department of Environmental Science, Policy, and Management, University of California, Berkeley, 117p.